A Concept for a Gas-Filter Correlation Radiometer to Remotely Sense the Atmospheric Carbon Dioxide Column from Space

BOYD T. TOLTON

Synodon, Inc., Edmonton, Alberta, Canada

9 May 2003 and 27 November 2003

ABSTRACT

Concern about the climatic effects of anthropogenic emissions of CO_2 has resulted in a growing need, both scientifically and politically, to monitor atmospheric CO_2. The development of a satellite instrument that could measure the global distribution of atmospheric CO_2 would greatly improve our understanding of the global carbon cycle and provide a means of monitoring regional sources and sinks. In this paper, the potential of a proposed nadir-viewing, satellite-based remote sounding instrument consisting of gas-filter correlation radiometers (GFCRs) tuned to the 6300- (1.6 μm) and 5000-cm^{-1} (2 μm) regions to globally measure the atmospheric CO_2 column is analyzed. Although the design of such an instrument would present some engineering challenges, the proposed instrument has significant potential. Such an instrument should be able to measure the atmospheric CO_2 column to a precision better than 1 ppmv.

1. Introduction

The anthropogenic emission of CO_2 has substantially altered the global carbon cycle and is expected to result in significant climate change. However, our ability to predict this change is significantly hampered by uncertainties in our understanding of the global budget of CO_2. It is estimated that approximately half of the anthropogenically emitted CO_2 remains in the atmosphere. The remaining half, often called the missing carbon, is sequestered by the oceans and the terrestrial biosphere (Houghton et al. 1990). Uncertainty in the strengths and effectiveness of these two sinks is a subject of considerable debate (Keeling et al. 1989; Tans et al. 1990; Francey et al. 1995). Recent studies into atmospheric isotopic carbon ratios and changes in the amplitude of the seasonal cycle of atmospheric carbon have suggested that the sinks are primarily associated with the terrestrial biosphere (Ciais et al. 1995; Fan et al. 1998; Keeling et al. 1996; Randerson et al. 1997; Zimov et al. 1999) However, without a good understanding of the fate of the missing carbon, predictions of future climate change will remain suspect.

Since preindustrial times, the concentration of CO_2 has increased by approximately 90 parts per million by volume (ppmv) to its present concentration of approximately 370 ppmv. Figure 1 shows the concentration of CO_2 measured at the South Pole; Mauna Loa, Hawaii; and Barrow, Alaska between 1974 and 2002, displaying spatial, seasonal, temporal, and trend variations (NOAA/CMDL/CCG 2003). These variations are a product of both the spatial and temporal variations in the natural and anthropogenic sources and sinks, and the atmospheric transport. Seasonal variations in CO_2, which are primarily a product of seasonal variation in the biological sinks, range from 1.5 ppmv (peak to peak) in the Southern Hemisphere to $>$20 ppmv in the high northern latitudes. Spatially, CO_2 is approximately 3–4 ppmv higher in the Northern Hemisphere than in the Southern Hemisphere, primarily due to higher anthropogenic emissions in the Northern Hemisphere (Denning et al. 1995). Between 1981 and 1992, CO_2 concentrations increased at a rate of approximately 1.43 ppmv per year (Conway et al. 1994).

Long-term observations of the global distribution of CO_2 concentrations are required to assess and understand the role of anthropogenic CO_2 in climate change (Wofsy and Harriss 2002). Currently, the most extensive and comprehensive long-term global CO_2 measurement program is operated by the National Oceanic and Atmospheric Administration's Climate Monitoring and Diagnostics Laboratory (NOAA/CMDL) global air sampling network. This program has provided surface and vertical profile measurements at various locations around the world starting in 1968 (Komhyr et al. 1985; Conway et al. 1994; NOAA/CMDL/CCG 2003). However, these measurements are limited and are not sufficient to provide a comprehensive understanding of spatial and temporal distributions and variations in the CO_2 budget (Park 1997).

Satellite-based remote sounding instruments capable

Corresponding author address: Dr. Boyd T. Tolton, Synodon, Inc., 6919 Roper Rd., Edmonton, AB T6B 3H9, Canada.
E-mail: boyd.tolton@synodon.com

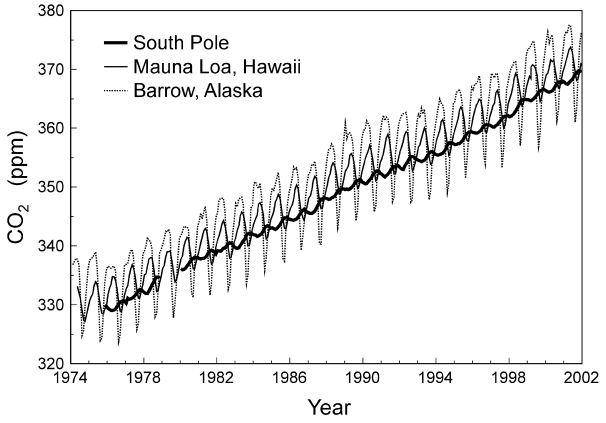

FIG. 1. Monthly mean atmospheric CO_2 mixing ratios at the South Pole; Mauna Loa, HI; and Barrow, AK from 1974 to 2002 (NOAA/CMDL/CCG 2003).

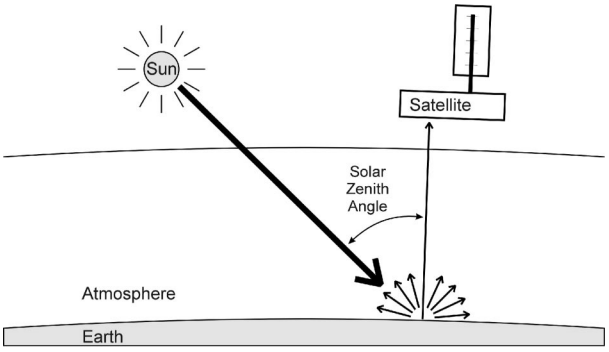

FIG. 2. A schematic showing the viewing geometry of the proposed GFCR satellite instrument to measure the atmospheric CO_2 column concentration. This nadir-viewing satellite instrument measures reflected solar radiation.

of measuring the long-term global distributions of CO_2 would greatly improve our ability to investigate the CO_2 budget. Although atmospheric CO_2 can be detected easily by remote sounding techniques, the accuracy and precision that are required to make scientifically useful measurements is difficult to achieve. This is due to the fact that the spatial and temporal variations in CO_2 concentrations are small relative to the total amount of CO_2 in the atmosphere. A recent paper by Rayner and O'Brien (2001) established that the required accuracy for column-integrated CO_2 concentrations must be better that 2.5 ppmv ($\approx$0.7%) on a $8^\circ \times 10^\circ$ footprint to provide comparable performance to existing surface measurements. Such a high accuracy requirement strongly influences the techniques and form of the measurement. In order to measure the atmospheric boundary layer, where the sources and sinks of CO_2 are located, an instrument must have a nadir or near-nadir view. Thus the instrument will measure the entire atmospheric column. Also, spatial variations in the surface pressure, reflectivity, and emissivity, along with variations in the vertical profile of temperature and the distribution of interfering gases, will add noise to the measurement. To minimize these noise sources, the measurements must be rapid, as the instantaneous field of view (IFOV) of the instrument will be moving quickly over the surface of the planet. And finally, the instrument must be capable of gathering enough energy to have a sufficient signal-to-noise ratio (SNR) to make the measurement.

Recently, a number of efforts have been made to analyze different remote sounding techniques to measure the atmospheric column of CO_2 from space (Aoki et al. 1993; Park 1997; Tolton and Plouffe 2001; Tolton et al. 2001; Kuze et al. 2001; O'Brien and Rayner 2002; Kuang et al. 2002; Yang et al. 2002). The techniques proposed have ranged between simple filter radiometers and Fourier transform spectrometers (FTSs). In this paper, I analyze the potential of a nadir-viewing gas-filter correlation radiometer (GFCR) tuned to the 6300- (1.6 μm) and 5000-cm^{-1} (2 μm) regions to measure the atmospheric CO_2 column. The viewing geometry of such an instrument is shown in Fig. 2. A GFCR is an instrument that uses a sample of the gas of interest as a spectral filter for the gas. It combines the advantages of the high-resolution spectral selectivity of a spectrometer with the energy grasp of a low-resolution radiometer. The principles of the GFCR being proposed are shown in Fig. 3. Incoming radiation is first passed through a narrow bandpass filter. The beam is then split by a beam splitter along two paths; one path containing a gas cell filled with the gas of interest (known as the correlation cell) and the other path containing no gas. The radiant flux in each path is then measured by infrared detectors, and the signals are analyzed. The difference in the transmission along the two paths corresponds primarily to the absorption of the gas along the correlation cell path. Two signals from the detectors can be defined: an average signal (S_{avg}) corresponding to the average radiant fluxes on the two detectors, and a difference signal (S_{diff}) corresponding to the difference in the radiant fluxes:

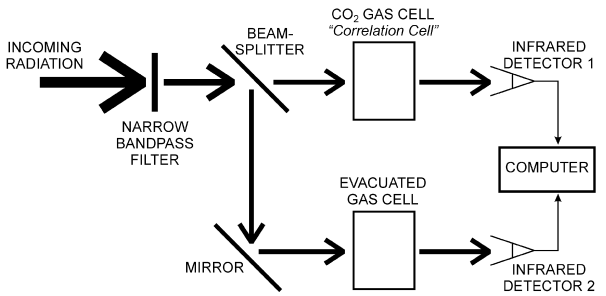

FIG. 3. A schematic showing the principles of GFCR. Incoming radiation is passed through a narrow bandpass filter and then split along two paths by a beam splitter. The two beams are then passed through two gas cells and the transmitted radiation is then measured by two detectors. Signals from the detectors are then analyzed using a computer.

$$S_{\text{avg}} = G \int_{\tilde{\nu}_1}^{\tilde{\nu}_2} I(\tilde{\nu})\tau_{\text{fil}}(\tilde{\nu})\left[\frac{\tau_{p1}(\tilde{\nu}) + \tau_{p2}(\tilde{\nu})}{2}\right] d\tilde{\nu} \quad \text{and} \quad (1)$$

$$S_{\text{diff}} = G \int_{\tilde{\nu}_1}^{\tilde{\nu}_2} I(\tilde{\nu})\tau_{\text{fil}}(\tilde{\nu})[\tau_{p1}(\tilde{\nu}) - \tau_{p2}(\tilde{\nu})]\, d\tilde{\nu}, \quad (2)$$

where G represents the instrument gain, $I(\tilde{\nu})$ is the radiant intensity incident on the radiometer, $\tau_{\text{fil}}(\tilde{\nu})$ is the transmission profile of the narrow bandpass filter with a bandpass region extending from $\tilde{\nu}_1$ to $\tilde{\nu}_2$, and $\tau_{p1}(\tilde{\nu})$ and $\tau_{p2}(\tilde{\nu})$ are the transmission functions of the two optical paths. The narrow bandpass filter is used to limit the detected radiation to wavenumbers corresponding to a spectral band of the gas. This significantly increases the depth of modulation S_{diff} relative to S_{avg}. Also, since a GFCR measures a band of lines, it can produce high SNR. In operation, it is often convenient to define an instrument signal from a GFCR as the ratio of the S_{diff} to the S_{avg}:

$$\frac{S_{\text{diff}}}{S_{\text{avg}}} = \frac{2\displaystyle\int_{\tilde{\nu}_1}^{\tilde{\nu}_2} I(\tilde{\nu})\tau_{\text{fil}}(\tilde{\nu})[\tau_{s1}(\tilde{\nu}) - \tau_{s2}(\tilde{\nu})]\, d\tilde{\nu}}{\displaystyle\int_{\tilde{\nu}_1}^{\tilde{\nu}_2} I(\tilde{\nu})\tau_{\text{fil}}(\tilde{\nu})[\tau_{s1}(\tilde{\nu}) + \tau_{s2}(\tilde{\nu})]\, d\tilde{\nu}}. \quad (3)$$

Defining it in this manner is convenient as, to first order, it removes the effects of the instrument gain and any broad absorption features (such as the surface reflectivity). Also, it is convenient as the $S_{\text{diff}}/S_{\text{avg}}$ ratio is a unitless value (or signal).

The choice to analyze the potential of a GFCR to measure the atmospheric CO_2 column was made for a number of reasons. First, it is a relatively simple instrument with few, if any, moving mechanisms, making it ideal for satellite-based applications. Second, it is capable of making quick measurements, making it ideal for nadir-viewing applications. Third, since the measurement is primarily radiometric, high SNRs can be achieved. This allows for measurements of diffusely reflected solar radiation from the sunlit side of the earth's surface, thus allowing the potential for measurements over the entire globe. Fourth, although the measurements of a GFCR are radiometric, it has very high spectral selectivity of the gas of interest. Consequently, unlike simple radiometers and more like spectrometers, GFCRs have minimal spectral interference by other gases. Fifth, it is a well-understood technology, as GFCRs have been used for over three decades in the remote sounding of the earth and other planets (Abel et al. 1970; Ellis et al. 1973; Drummond et al. 1980; Reichle et al. 1986, 1990, 1999; Tolton and Drummond 1999).

For this analysis, the 6300- (1.6 μm) and 5000-cm^{-1} (2 μm) bands of CO_2 were chosen, as a number of relatively ''weak'' absorption bands of CO_2 are located within these regions, with very little radiometric interference by other gases (principally water vapor). Also, for a nadir-viewing satellite tuned to these bands, the upwelling radiation on the sunlit side of the earth is primarily reflected solar radiation. This minimizes the sensitivity to radiative emissions from the surface and atmosphere (thus a pure transmission experiment) and maximizes the sensitivity to CO_2 near the surface (due to the radiative contrast). A calculated atmospheric CO_2 transmission spectra plus the spectra of other interfering atmospheric species for the 6300- and 5000-cm^{-1} CO_2 bands are shown in Figs. 4a–c and 5a–c, respectively. Figures 4d and 5d show the combined transmission spectra of each band.

The intent of this research is to analyze the potential of a GFCR to measure the atmospheric CO_2 column from a satellite. I have not attempted to fully define and characterize a complete satellite GFCR instrument. Nor have I attempted to determine the optimal design and/or configuration of the GFCR. A complete analysis of this technique as well as other remote sensing techniques should be performed to determine which will provide the most effective measurements.

2. Calculation of radiometric sensitivities

Although CO_2 can easily be detected by remote sounding techniques, the precision required to make scientifically useful measurements is difficult to achieve. Indeed, variations in the column amount of CO_2 due to changes in the surface pressure are much larger than natural variations due to sources and sinks. The form and type of the GFCR required to measure CO_2 in the 6300- and 5000-cm^{-1} bands are strongly influenced by the fact that these absorption bands are very weak. In designing a GFCR, it is desirable to have the absorptions lines of the gas in the correlation cell approximately of the same width as the lines in the atmosphere. Therefore, for my calculations, I chose a correlation cell pressure of 100 kPa. Since these bands are nearly saturated in the atmosphere, making the absorption lines narrower by reducing the pressure in the correlation cell would just reduce your sensitivity. However, increasing the pressure would increase the width of the absorption lines in the correlation cell and, therefore, increase the sensitivity to spectral interference by other gases. It is also desirable in designing a GFCR to have the strong absorption by the gas in the correlation cell, thus maximizing the S_{diff}. Unfortunately, due to fact that these bands are very weak, this requires very long correlation cell pathlengths. For the 6300-cm^{-1} bands, I have chosen to analyze a correlation cell with a pathlength of CO_2 of 10.0 m and a pressure of 100 kPa. For the 5000-cm^{-1} band, since this band is stronger, I chose a correlation cell with a pathlength of CO_2 of 2.0 m and a pressure of 100 kPa. These correlation cell lengths were chosen because they produce reasonably strong absorptions, as shown in Fig. 4e (6300 cm^{-1}) and Fig. 5e (5000 cm^{-1}). Such long pathlengths preclude the implemen-

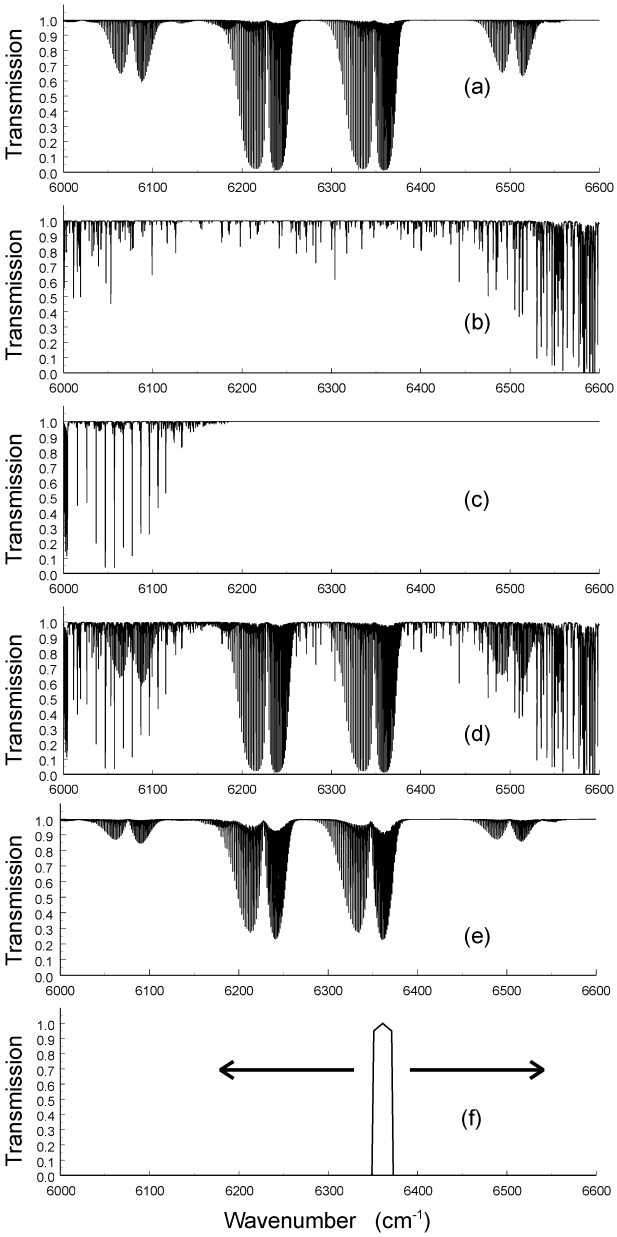

FIG. 4. Plots showing calculated atmospheric transmission spectra in the 6000–6600-cm^{-1} range of (a) CO_2, (b) H_2O, (c) CH_4, (d) all, (e) the transmission of a 10-m-long gas cell filled with 100 kPa of CO_2, and (f) the transmission profile of a 22-cm^{-1} narrow bandpass filter used in this work. This calculation assumed a *U.S. Standard Atmosphere* (temperature and pressure), a CO_2 concentration of 370 ppmv, a relative humidity of 70% in the troposphere, and a solar zenith angle (SZA) of 30°.

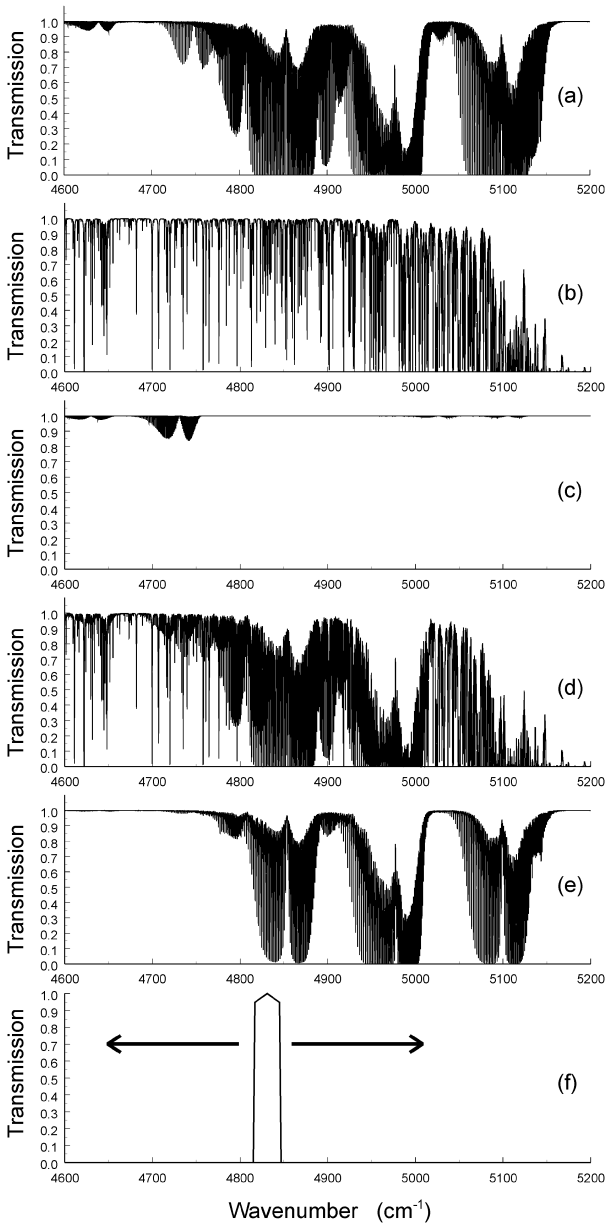

FIG. 5. Plots showing calculated atmospheric transmission spectra in the 4600–5200-cm^{-1} range of (a) CO_2, (b) H_2O, (c) N_2O, (d) all, (e) the transmission of a 2-m-long gas cell filled with 100 kPa of CO_2, and (f) the transmission profile of a 30 cm^{-1} narrow bandpass filter used in this work. This calculation assumed a *U.S. Standard Atmosphere* (temperature and pressure), a CO_2 concentration of 370 ppmv, a relative humidity of 70% in the troposphere, and an SZA of 30°.

tation of some commonly used GFCR forms, such as pressure modulator radiometers (PMRs) and length modulated radiometer (LMRs) (Taylor 1983; Drummond et al. 1980; Tolton and Drummond 1999). Instead the form of GFCR I am proposing is similar in concept to that used in the the Measurement of Air Pollution from Satellites (MAPS) satellite instrument, consisting of static correlation cells (see Fig. 3) (Reichle et al. 1986, 1990, 1999). Undoubtedly, such a long pathlength will complicate the engineering and design of a satellite instrument. However, such pathlengths should be should be achievable within a reasonable instrument size using multipass cells.

To analyze the potential of such a GFCR to measure the atmospheric CO_2 column, I have performed a series

TABLE 1. Parameters used in the calculation of the response of the GFCR.

Calculation parameters		Atmospheric parameters	
Resolution	0.005 cm^{-1}	Height of atmosphere	40 km
Wing cutoff	$\geq$20 cm^{-1}	Atmospheric shell thickness	1 km
Bandpass filters	22 cm^{-1} wide at 6300 cm^{-1} (Fig. 4f)	Solar zenith angle	30°
	30 cm^{-1} wide at 5000 cm^{-1} (Fig. 5f)	Temperature and pressure profile	*U.S. Standard Atmosphere*
	42 cm^{-1} wide at 13 100 cm^{-1} (Fig. 17d)		
Spectral range	Filter limits $\pm$ cutoffs	Surface pressure	101.325 kPa
Spectral line data	Hitran 2000 (Rothman et al. 1998)	Interfering gases	H_2O, CH_4, and N_2O
		CO_2 concentration	370-ppmv constant column
		H_2O concentration profile	70% RH troposphere
		CH_4 concentration	1.7-ppmv constant column
		N_2O concentration profile	300-ppbv constant column
		Solar source function	5780-K blackbody

of radiometric sensitivity calculations. The results of these calculations are presented in the next five subsections. Section 2a details the sensitivity of the proposed GFCRs to the atmospheric CO_2 column concentration (i.e., it shows how the GFCR signals change as a function of the CO_2 column concentration). Sections 2b and 2c detail the sensitivity to uncertainty in the atmospheric temperature, humidity, and nitrous oxide (N_2O) concentration. Section 2d details the sensitivity to uncertainty in the surface altitude (or surface pressure). And finally, section 2e details the sensitivity to the spectral width of the narrow bandpass filter used in the GFCRs. These calculations assumed a 22 cm^{-1} wide nominal narrow bandpass filter for the 6300-cm^{-1} band and a 30 cm^{-1} wide nominal narrow bandpass filter for the 5000-cm^{-1} band (Figs. 4f and 5f). These profile widths were chosen so as to cover one branch of the CO_2 absorption bands, thus providing near maximal sensitivity to CO_2. The nominal calculation parameters of the atmosphere, the instrument, and the calculations used in this analysis are listed in Table 1. The values calculated are the changes in the measured S_{diff}/S_{avg} signal (unitless) as a function of a variable (e.g., as a function of the surface pressure). The results of these calculations are summarized in Tables 2 and 3.

a. Sensitivity to the atmospheric CO_2 column

An analysis of the sensitivity of a GFCR instrument to the atmospheric CO_2 concentration for the 6300- (1.6 μm) and 5000-cm^{-1} (2 μm) bands of CO_2 was performed and the results are shown later [in Figs. 6 and 8 (thick solid line), respectively]. This analysis calculated the change in the S_{diff}/S_{avg} signal per ppmv change in the CO_2 column concentration (change from 370 ppmv nominal), as a function of the position of a narrow bandpass filter. It shows that the peak sensitivity to CO_2 in the 6300-cm^{-1} band occurs with a filter centered in the R branches, with a maximum sensitivity (i.e., change in the S_{diff}/S_{avg} signal) of approximately -7×10^{-5} per ppmv of CO_2 (Fig. 6). For the 5000-cm^{-1} bands, peak sensitivities of the two bands that are located in this region are approximately -6×10^{-4} $ppmv^{-1}$ of CO_2 (at 4990 cm^{-1}) and -1.5×10^{-4} $ppmv^{-1}$ of CO_2 (at 4840 cm^{-1}) (Fig. 8). The change in the S_{diff}/S_{avg} signal as a function of the CO_2 concentration is negative as an increase in the atmospheric CO_2 will reduce the energy detected at the absorption lines of CO_2 and therefore reduce the S_{diff} signal.

b. Sensitivity to changes in atmospheric temperature, humidity, and N_2O concentration

The sensitivity of a GFCR measurement of the atmospheric CO_2 column to interference by changes in the temperature, the water content of the atmosphere, and the N_2O concentration of the atmosphere are shown in Figs. 6–10. The change in the S_{diff}/S_{avg} signal as a function of the change in the atmospheric temperature and the position of a narrow bandpass filter for the 6300-

TABLE 2. Sensitivities of the proposed GFCR.

	CO_2 sensitivity	Surface altitude sensitivity		Temperature sensitivity		Water vapor sensitivity	
Channel	Change in S_{diff}/S_{avg} (per ppmv CO_2)	Change in S_{diff}/s_{avg} (per m or kPa)	Equivalent change* (m or kPa)	Change in S_{diff}/S_{avg} (per °C)	Equivalent change* (°C)	Change in S_{diff}/S_{avg} (per % RH)	Equivalent change* (% RH)
CO_2 (6367 cm^{-1})	-6.24×10^{-5}	2.89×10^{-6} m^{-1}	21.6 m	8.30×10^{-7}	75	1.1×10^{-6}	56
		-2.64×10^{-4} kPa^{-1}	-0.254 kPa				
CO_2 (4831 cm^{-1})	-1.16×10^{-4}	8.56×10^{-6} m^{-1}	13.5 m	-1.85×10^{-6}	63	-8.84×10^{-6}	13
		-7.29×10^{-4} kPa^{-1}	-0.159 kPa				
O_2 (13 158 cm^{-1})	0	4.25×10^{-4} per 20 m	—	7.1×10^{-6}	60	0	—

* Equivalent change represents the change in a parameter required to produce an equivalent change in the S_{diff}/S_{avg} signal to that caused by either a 1-ppmv change in the CO_2 concentration (for the CO_2 channels) or a 20-m change in the surface altitude (for the O_2 channel).

TABLE 3. Properties of the sun, the earth's surface, and the hypothetical satellite instrument used in the calculation of the instrument sensitivities.

Environmental properties		Instrument properties	
Solid angle of sun	6.8×10^{-5} sr	Satellite altitude	700 km
Temperature of sun	5780 K	Surface resolution	20 km diam
Zenith angle	30°	Observation time	0.5 s
Surface reflectivity	10%	Collector diameter	8 cm
Diffusivity	Lambertian	A–Ω product	3.22×10^{-6} m^2 sr
		Radiometer transmission	90%
		Detector size	1-mm diam
		Detector D*	2×10^{12} cm Hz$^{0.5}$ W^{-1}

and 5000-cm^{-1} bands of CO_2 are shown in Figs. 6 and 8 (thin solid line), respectively. This analysis shows that minimums in the sensitivity to atmospheric temperature changes occur in the middle of the P and R branches, near the regions of maximum CO_2 sensitivity. The change in the $S_{\text{diff}}/S_{\text{avg}}$ signal as a function of the change in the atmospheric relative humidity (RH) and the position of a narrow bandpass filter for the 6300- and 5000-cm^{-1} bands of CO_2 are shown in Figs. 7 and 9 (thin solid line), respectively. As expected, due to the spectral selectivity of the GFCR technique, this analysis shows minimum sensitivity to interference by water vapor in the 6300-cm^{-1} bands. For the 5000-cm^{-1} bands, since the absorption by water vapor is much stronger in these bands, only a few regions of minimal interference exist. The change in the $S_{\text{diff}}/S_{\text{avg}}$ signal as a function of the change in the atmospheric N_2O concentration and the position of a narrow bandpass filter for 5000-cm^{-1} bands of CO_2 are shown in Fig. 10 (thin solid line). Interference by N_2O is only an issue for the 5000-cm^{-1} bands of CO_2. Also as expected, the GFCR technique minimizes N_2O interference. The dotted lines in Figs. 6–10 show the (magnitude of a) change in atmospheric temperature, water vapor, and N_2O concentration required

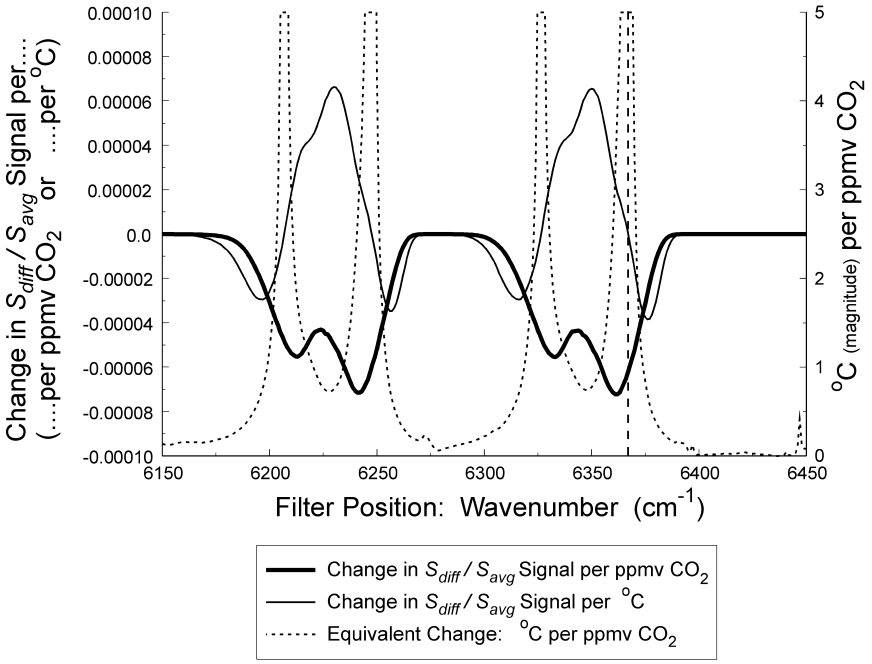

FIG. 6. Plot showing the change in the $S_{\text{diff}}/S_{\text{avg}}$ signal in the 6150–6450-cm^{-1} range as a function of (i) a 1-ppmv change in the atmospheric CO_2 concentration (thick solid line, left axis), and (ii) a 1°C change in the atmospheric temperature (thin solid line, left axis), all as a function of the narrow bandpass filter position. Also shown is the required change in the atmospheric temperature (magnitude) to produce a change in the $S_{\text{diff}}/S_{\text{avg}}$ signal equivalent to that produced by a 1-ppmv change in the CO_2 concentration (dotted line, right axis), also as a function of the narrow bandpass filter position (i.e., the ''equivalent change''). This figure highlights spectral regions of minimum temperature sensitivity located in regions of strong sensitivity to changes in the CO_2 concentration. The vertical dashed line highlights the position of a narrow bandpass filter at 6367 cm^{-1} used to calculate the vertical sensitivity to CO_2, to temperature, and to the surface altitude/pressure of a CO_2 GFCR.

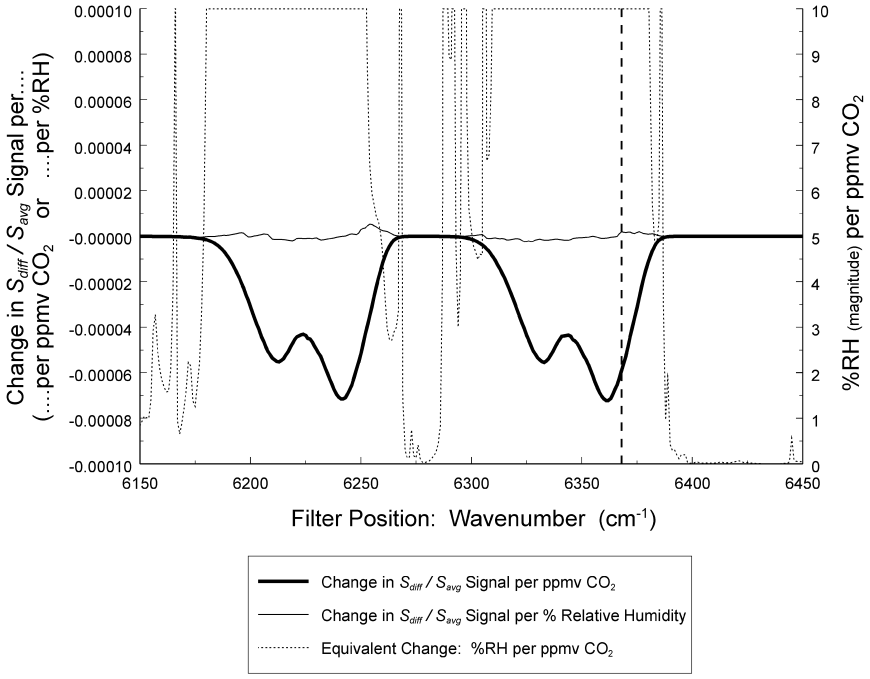

FIG. 7. Plot showing the change in the S_{diff}/S_{avg} signal in the 6150–6450-cm^{-1} range as a function of (i) a 1-ppmv change in the atmospheric CO_2 concentration (thick solid line, left axis) and (ii) a 1% change in the atmospheric relative humidity (thin solid line, left axis), all as a function of the narrow bandpass filter position. Also shown is the required change in the atmospheric relative humidity (magnitude) to produce a change in the S_{diff}/S_{avg} signal equivalent to that produced by a 1-ppmv change in the CO_2 concentration (dotted line, right axis), also as a function of the narrow bandpass filter position (i.e., the equivalent change). This figure highlights minimum water vapor sensitivity located in regions of strong sensitivity to changes in the CO_2 concentration.

to produce a change in the S_{diff}/S_{avg} signal equivalent to that produced by a 1-ppmv change in the CO_2 concentration (i.e., the ''equivalent change''), also as a function of the narrow bandpass filter position. These curves highlight the regions of minimum sensitivity to interference. Therefore, by selecting an appropriate filter position, the GFCR measurement of the atmospheric CO_2 column can minimize sensitivity to interference by changes in atmospheric temperature, water vapor, and N_2O.

c. Sensitivity to atmospheric CO_2 and temperature as a function of altitude

Calculation of the sensitivity of GFCR measurements of the atmospheric CO_2 column to changes in the CO_2 concentration as a function of altitude for the 6300- and 5000-cm^{-1} bands of CO_2 has been performed, and the results are shown in Figs. 11 and 12 (circles), respectively. These calculations were performed for narrow bandpass filters located at 6367 and 4831 cm^{-1} in regions of minimum temperature sensitivity and minimum water vapor and N_2O interference, as calculated in the previous section. These filter positions are highlighted by the vertical dashed lines in Figs. 6–10. These data show the change in the S_{diff}/S_{avg} signal as a function of a 1-ppmv increase in the CO_2 concentration in each 1-km layer of the atmosphere. As expected, it shows that the peak sensitivity to mixing ratio changes in the CO_2 concentration is at the surface. Figure 13 shows the change in the S_{diff}/S_{avg} signal as a function of a one CO_2 molecule cm^{-2} increase in CO_2 column density in each 1-km layer of the atmosphere, for both the 6367- and 4831-cm^{-1} GFCRs. These data show that the peak sensitivity to atmospheric CO_2 occurs in the midtroposphere for the 6367-cm^{-1} GFCR and at the surface for the 4831-cm^{-1} GFCR. These results suggest the possibility of achieving vertical profile information about atmospheric CO_2 from a multichannel GFCR instrument.

A calculation of the sensitivity of the same GFCR measurement of the atmospheric CO_2 column to changes in the atmospheric temperature as a function of altitude for the 6300- and 5000-cm^{-1} bands of CO_2 has been performed, and is shown in Figs. 11 and 12 (triangles). These figures shows that the sensitivity to the vertical temperature structure is small, with the peak sensitivity per degree Celsius at the surface and approximately 7 or 8 times smaller than the sensitivity per ppmv of CO_2.

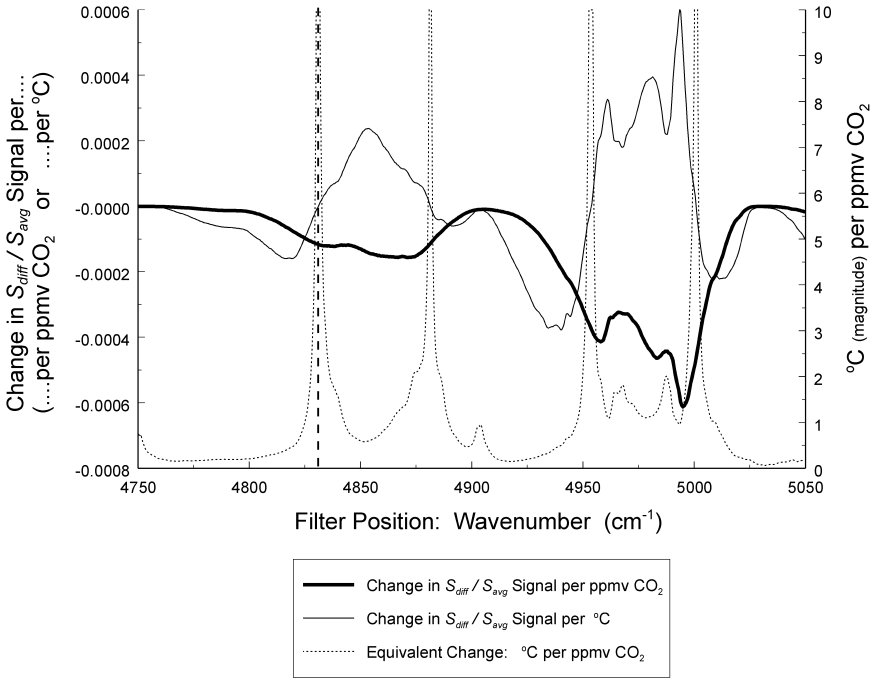

FIG. 8. Plot showing the change in the S_{diff}/S_{avg} signal in the 4750–5050-cm^{-1} range as a function of (i) a 1-ppmv change in the atmospheric CO_2 concentration (thick solid line, left axis), and (ii) a 1°C change in the atmospheric temperature (thin solid line, left axis), all as a function of the narrow bandpass filter position. Also shown is the required change in the atmospheric temperature (magnitude) to produce a change in the S_{diff}/S_{avg} signal equivalent to that produced by a 1-ppmv change in the CO_2 concentration (dotted line, right axis), also as a function of the narrow bandpass filter position (i.e., the equivalent change). This figure highlights spectral regions of minimum temperature sensitivity located in regions of strong sensitivity to changes in the CO_2 concentration. The vertical dashed line highlights the position of a narrow bandpass filter at 4831 cm^{-1} used to calculate the vertical sensitivity to CO_2, to temperature, and to the surface altitude/pressure of a CO_2 GFCR.

d. Sensitivity to surface pressure/altitude

Analyses of the sensitivity of GFCR measurements of the atmospheric CO_2 column to changes in the surface pressure and/or surface altitude for the 6300- and 5000-cm^{-1} bands of CO_2 have been performed, and are shown in Figs. 14 and 15. These figures show the change in the measured S_{diff}/S_{avg} signal as a function of the surface altitude (panel a) and the surface pressure (panel b), for the same GFCRs studied in section 2c (i.e., with the 6367- and 4831-cm^{-1} narrow bandpass filters). Given that the sensitivity to the changes in the atmospheric CO_2 column (i.e., the change in the S_{diff}/S_{avg} signal per ppmv of CO_2) is -6.24×10^{-5} $ppmv^{-1}$ for the 6367-cm^{-1} GFCR and that the sensitivity to the surface altitude (pressure) is 2.89×10^{-6} m^{-1} (-2.46×10^{-4} kPa^{-1}), the required knowledge of the surface altitude (pressure) over the viewed pixel is 21.6 m (0.254 kPa). Similarly, since the sensitivity to the changes in the atmospheric CO_2 column is -1.16×10^{-4} $ppmv^{-1}$ for the 4831-cm^{-1} GFCR and that the sensitivity to the surface altitude (pressure) over the viewed pixel is 8.56×10^{-6} m^{-1} (-7.29×10^{-4} kPa^{-1}), the required knowledge of the surface altitude (pressure) is 13.5 m (0.159 kPa).

e. Sensitivity to the narrow bandpass filter width

An analysis of the sensitivity of GFCR measurements to the width of the narrow bandpass filter profiles has been performed and the results are shown in Fig. 16. This figure shows the sensitivity of the GFCR to CO_2 and the equivalent change of temperature for the 6300-cm^{-1} CO_2 bands, for filter widths of 10 (dashed lines) and 38 cm^{-1} (solid lines). It demonstrates that although the sensitivity of the GFCR to CO_2 is reduced by increasing the width of the filter profile, the region of minimum temperature sensitivity (i.e., an equivalent change of atmospheric temperature of $\geq$10°C) is increased. Also, increasing the filter profile width would result in an increase in the total energy gathered by the GFCR, thus increasing the SNR. This result allows flexibility in the design and engineering of a GFCR instrument. In designing an instrument, a trade-off study would be required to determine the operationally optimal filter width.

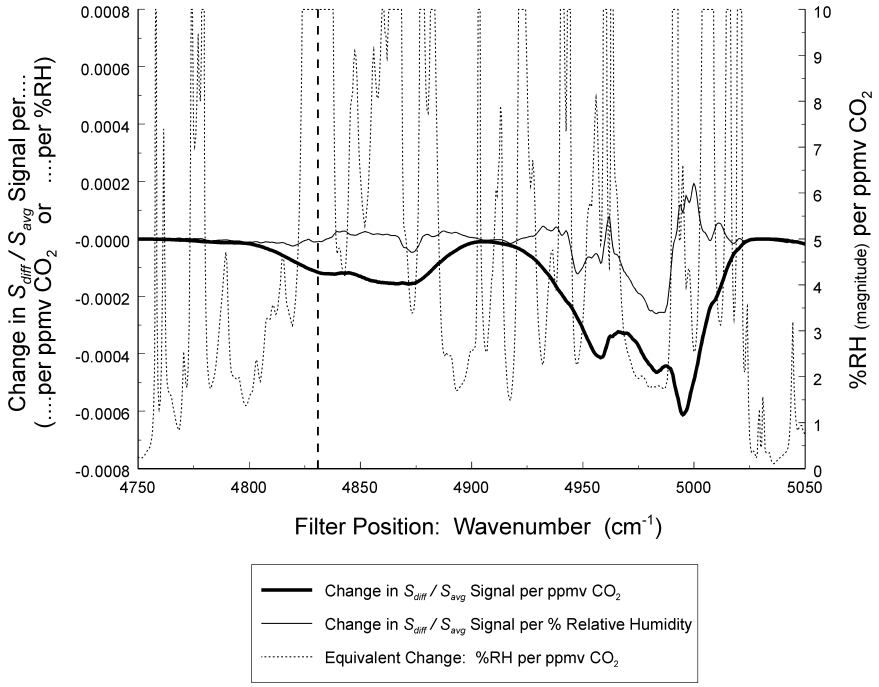

FIG. 9. Plot showing the change in the S_{diff}/S_{avg} signal in the 4750–5050-cm^{-1} range as a function of (i) a 1-ppmv change in the atmospheric CO_2 concentration (thick solid line, left axis) and (ii) a 1% change in the atmospheric relative humidity (thin solid line, left axis), all as a function of the narrow bandpass filter position. Also shown is the required change in the atmospheric relative humidity (magnitude) to produce a change in the S_{diff}/S_{avg} signal equivalent to that produced by a 1-ppmv change in the CO_2 concentration (dotted line, right axis), also as a function of the narrow bandpass filter position (i.e., the equivalent change). This figure highlights minimum water vapor sensitivity located in regions of strong sensitivity to changes in the CO_2 concentration.

3. Determination of the total atmospheric column

In order to measure the column-averaged mixing ratio of CO_2 in the atmosphere, knowledge of the total column amount of the atmosphere is required. In section 2d, it was determined that required accuracy, expressed in terms of the surface pressure, is 0.254 kPa (≈20 m altitude) for the 6367-cm^{-1} GFCR and 0.159 kPa (≈13 m altitude) for the 4831-cm^{-1} GFCR. In operation, this level of accuracy in the knowledge of the surface pressure might easily be provided by weather forecast and surface terrain height models. However, it is still likely that any satellite measurements of the CO_2 column would require an ancillary channel or instrument not only to measure the surface pressure, but to assess the cloudiness of the FOV. In order to measure the surface pressure, it is necessary to measure a different gas with a known and stable concentration. I have selected the oxygen (O_2) A band at 13 100 cm^{-1} (760 nm). This band, shown in Fig. 17, like the 6300-cm^{-1} CO_2 bands, is a relatively strong absorption band in a region of minimal spectral interference by water vapor. Retrievals of the surface pressures from spectroscopic measurements of the O_2 A band to an accuracy of 0.1% have been demonstrated (O'Brien et al. 1998).

Like the CO_2 bands, the O_2 A band has relatively weak line strengths. Therefore, to measure O_2 by a GFCR technique also requires long correlation cell pathlengths. However, since the O_2 A-band spectra of the atmosphere are very strongly saturated at line centres, very high pressures of O_2 are required in the correlation cell to widen the absorption lines so as to provide sensitivity to the O_2 column. Consequently, I have chosen to analyze a GFCR with a pathlength of 10 m and a pressure of 1000 kPa (≈10 atm). The absorption spectra of the O_2 correlation cell are shown in Fig. 17c. The narrow bandpass filter profile is shown in Fig. 17d, with an assumed width of 42 cm^{-1} (a width of 0.32% of filter position). Figure 18 shows the change in the S_{diff}/S_{avg} signal as a function of a 20-m change in the surface altitude, all as a function of the narrow bandpass filter position (thick solid line). This figure shows that the peak change in the S_{diff}/S_{avg} signal is around 6×10^{-4} per 20-m surface altitude.

Similar to the CO_2, the O_2 GFCR measurement is sensitive to changes in the atmospheric temperature. Figure 18 also shows the change in the S_{diff}/S_{avg} signal as a function of 1°C change in the atmospheric temperature, all as a function of the narrow bandpass filter position (thin solid line). The dotted line shows the required change in the atmospheric temperature (magnitude) to produce a change in the S_{diff}/S_{avg} signal equivalent to that produced by a 20-m change in the surface

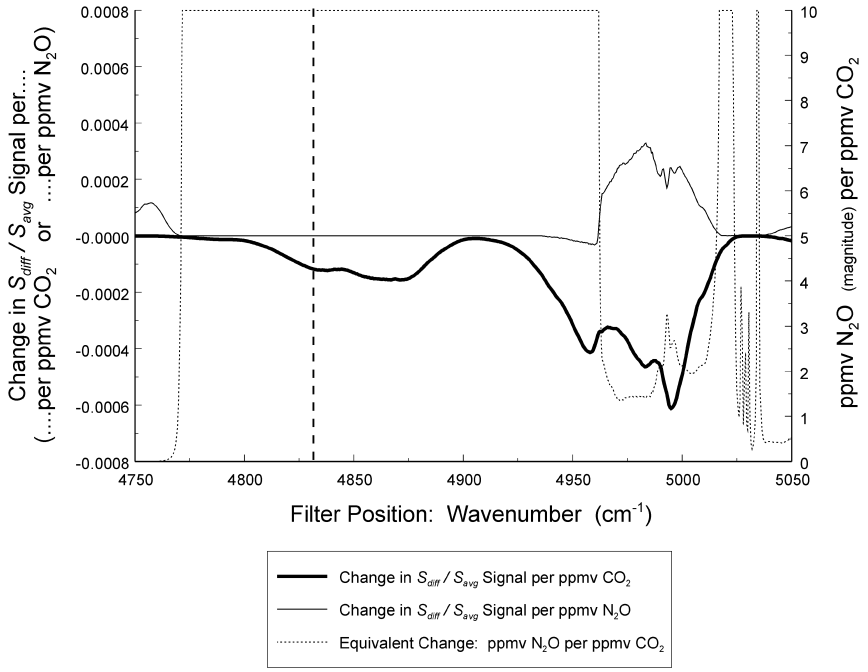

FIG. 10. Plot showing the change in the S_{diff}/S_{avg} signal in the 4750–5050-cm^{-1} range as a function of (i) a 1-ppmv change in the atmospheric CO_2 concentration (thick solid line, left axis) and (ii) a 1-ppmv change in the atmospheric N_2O concentration (thin solid line, left axis), all as a function of the narrow bandpass filter position. Also shown is the required change in the atmospheric N_2O concentration (magnitude) to produce a change in the S_{diff}/S_{avg} signal equivalent to that produced by a 1-ppmv change in the CO_2 concentration (dotted line, right axis), also as a function of the narrow bandpass filter position (i.e., the equivalent change). This figure highlights minimum N_2O sensitivity located in regions of strong sensitivity to changes in the CO_2 concentration.

altitude, also as a function of the filter position (i.e., the ''equivalent change''). This highlights the regions with minimum sensitivity to temperature changes. Similarly, by selecting the position of the filter profile, such as 13 158 cm^{-1}, the measurement of the total column of O_2 can minimize the sensitivity to interference by changes in the atmospheric temperature. The results of these calculations are summarized in Table 2.

4. Estimates of instrument sensitivities

In sections 2 and 3 I have calculated the required radiometric sensitivities of hypothetical CO_2 and O_2 GFCRs to measure the atmospheric CO_2 and O_2 columns. In order to determine whether these sensitivities are achievable, I have performed a series of simple calculations of the noise equivalent power (NEP, optical input power to the detector that produces SNR of unity) and radiometrics of the hypothetical GFCR instruments. The assumptions used in these calculations about the sun, the earth's surface, and the instrument are listed in Table 3. The sun was modeled as a 5780-K blackbody source, illuminating the earth's surface at a solar zenith angle of 30°. The surface was assumed to be a 10% reflective Lambertian surface. The instrument was assumed to be in a 700-km-altitude orbit with a surface resolution (FOV) of 20 km and have an observation time of 0.5 s. The collector optic was assumed to have a diameter of 8 cm, resulting in an A–Ω product of 3.22 $\times 10^{-6}$ m^2 sr. The instrument transmission was assumed to be 90% and the detectivity D* of the detectors was assumed to be 2×10^{12} cm $Hz^{0.5}$ W^{-1}. The calculated powers of the S_{avg} and S_{diff} signals for each GFCR are listed in Table 4 and are approximately 80 and 10 nW, respectively. The calculated NEP is 7.9×10^{-14} W, resulting in a noise-to-signal ratio (NSR, the inverse of SNR) for the S_{diff}/S_{avg} signals of $\approx 10^{-5}$ (SNR $\approx$ 100 000). For the 6367-cm^{-1} CO_2 channel, this ratio is a factor of 7 times lower than the required sensitivity to measure the CO_2 column to a precision of 1 ppmv. For the 4831-cm^{-1} CO_2 channel, this ratio is a factor of 12 times lower than the required sensitivity to measure the CO_2 column to a precision of 1 ppmv. For the 13 158 cm^{-1} O_2 channel, this ratio is a factor of 28 times lower than the required sensitivity to measure the surface altitude to a precision of 20 m. Consequently, the sensitivities of the proposed GFCRs are not instrument limited. The results of these calculation are summarized in Table 4. For reference purposes, the calculated SNR ratios for the CO_2 GFCR(s) are comparable to those of the Measurements Of Pollution In The Troposphere

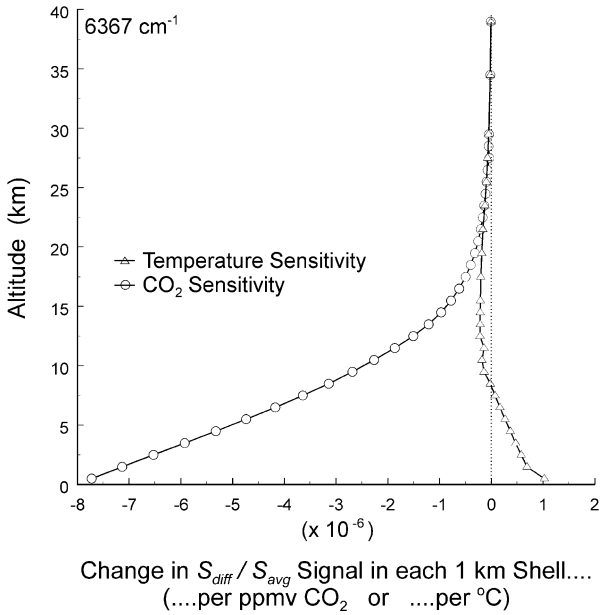

FIG. 11. Sensitivity of a GFCR measurement of atmospheric CO_2 tuned to the 6367-cm^{-1} region to changes in the vertical profile of atmospheric CO_2 and temperature. Plot shows the change in the S_{diff}/S_{avg} signal as a function of a 1-ppmv change in the CO_2 concentration in each 1-km layer of the atmosphere (circles), and as a function of a 1°C change in the temperature in each 1-km layer of the atmosphere (triangles).

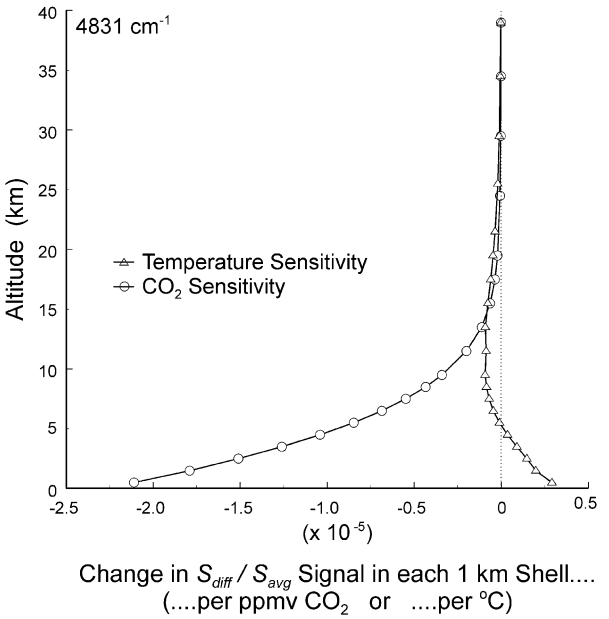

FIG. 12. Sensitivity of a GFCR measurement of atmospheric CO_2 tuned to the 4831-cm^{-1} region to changes in the vertical profile of atmospheric CO_2 and temperature. Plot shows the change in the S_{diff}/S_{avg} signal as a function of a 1-ppmv change in the CO_2 concentration in each 1-km layer of the atmosphere (circles), and as a function of a 1°C change in the temperature in each 1-km layer of the atmosphere (triangles).

(MOPITT), the last major GFCR remote sensing satellite instrument (Drummond et al. 1993).

It should be noted that these calculations are based on the simple conceptual design of GFCR that I used in previous calculations. The SNR ratio of the instrument could be easily improved by many means, such as increasing the width of the filter profile. This would greatly increase the energy gathered by the GFCR (i.e., the signal) without significantly reducing the sensitivity to CO_2 or increasing the sensitivity to temperature, as shown in section 2e. Consequently, a sensitivity to the atmospheric CO_2 column below 1 ppmv may be achievable.

5. Estimates of the hypothetical CO_2 and O_2 GFCR resolutions

The previous analysis has shown that the careful placement of the narrow bandpass filter profiles will minimize the sensitivity to interference due to atmospheric temperature and water vapor variations, while maintaining a strong sensitivity to either the atmospheric CO_2 or O_2 column. Based on the calculated sensitivities, I have estimated the overall instrument resolutions of the hypothetical CO_2 and O_2 GFCRs. These overall estimates are based on estimates of the maximum systematic errors in atmospheric temperature (10°C), water vapor (10% RH), and surface altitude (10 m), plus the instrument noise. Also, they assume that the errors in

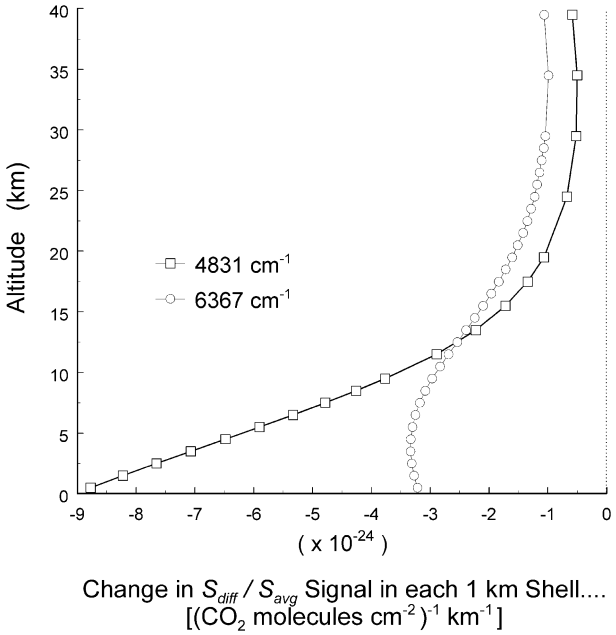

FIG. 13. Sensitivity of a GFCR measurement of atmospheric CO_2 tuned to the 6367- and 4831-cm^{-1} regions to changes in the vertical profile of atmospheric CO_2. Plot shows the change in the S_{diff}/S_{avg} signal as a function of a 1 CO_2 molecule per cm^2 change in the CO_2 density in each 1-km layer of the atmosphere.

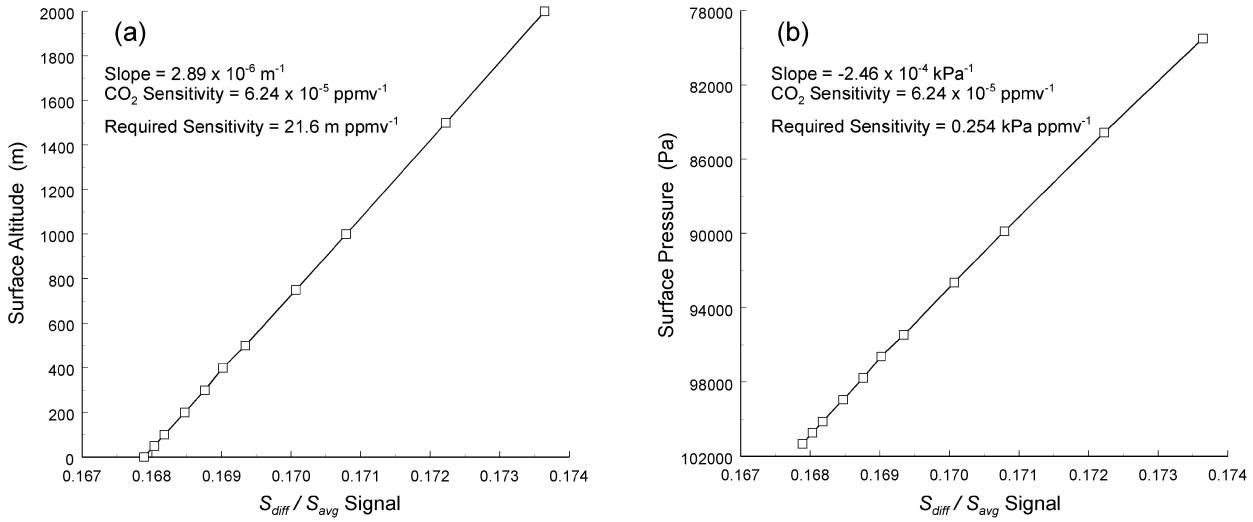

FIG. 14. Sensitivity of a GFCR measurement of atmospheric CO_2 tuned to the 6367-cm^{-1} region to changes in the surface altitude and pressure. Plot shows the S_{diff}/S_{avg} signal as a function of (a) the surface altitude (m ASL) and (b) the surface pressure. Given that the calculated change in the S_{diff}/S_{avg} signal produced by a 1-ppmv change in the CO_2 concentration is 6.24×10^{-5}, the surface altitude and pressure must be known to an accuracy of 21.6 m and 0.254 kPa in order to measure the CO_2 concentration to an precision of 1 ppmv.

these parameters are random and independent of each other, and that any other bias errors could be removed during the validation process. The results of these estimates are shown in Table 5. The overall estimated measurement resolutions for the 6367- and 4831 cm^{-1} CO_2 GFCRs are 0.53 and 1.1 ppmv, respectively. The overall estimated measurement resolution for the 13 158-cm^{-1} O_2 GFCR is 0.87-m altitude.

6. Summary

The anthropogenic release of CO_2 has significantly altered the global carbon cycle during the last century, and is expected to significantly influence the future climate of the earth. As such, the sources, sinks, and transport of CO_2 are of great scientific interest. A satellite-based remote sounding instrument capable of measuring

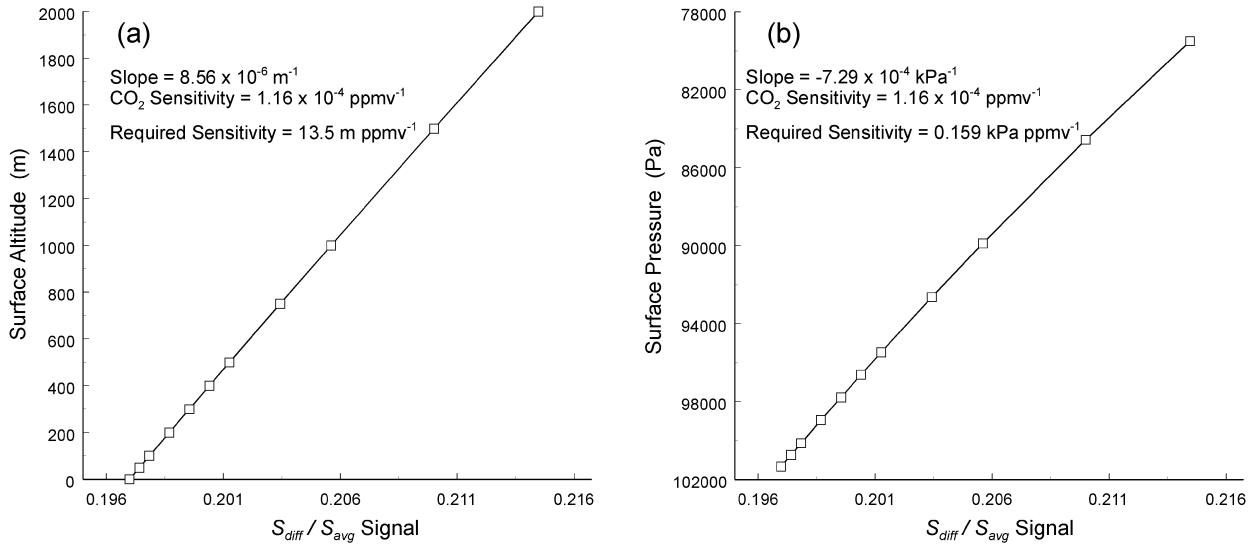

FIG. 15. Sensitivity of a GFCR measurement of atmospheric CO_2 tuned to the 4831-cm^{-1} region to changes in the surface altitude and pressure. Plot shows the S_{diff}/S_{avg} signal as a function of (a) the surface altitude (m ASL) and (b) the surface pressure. Given that the calculated change in the S_{diff}/S_{avg} signal produced by a 1-ppmv change in the CO_2 concentration is 1.16×10^{-4}, the surface altitude and pressure must be known to an accuracy of 13.5 m and 0.159 kPa in order to measure the CO_2 concentration to an precision of 1 ppmv.

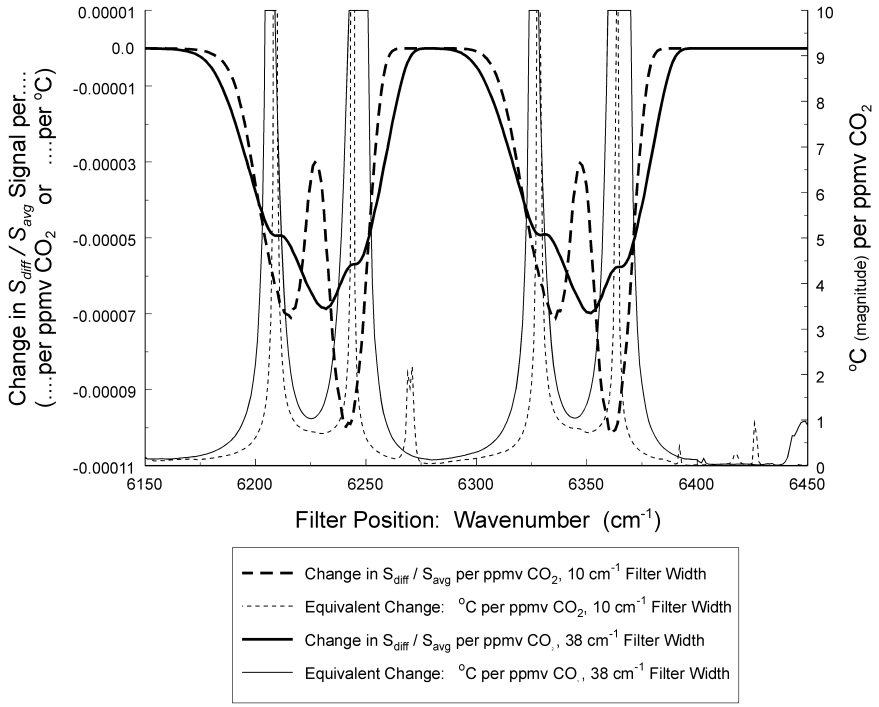

FIG. 16. Plot showing the change in the S_{diff}/S_{avg} signal in the 6150–6450-cm^{-1} range as a function of a 1-ppmv change in the atmospheric CO_2 concentration (thick lines, left axis) as a function of the narrow bandpass filter position, for two filter widths of 10 (dashed lines) and 38 cm^{-1} (solid lines). Also shown is the required change in the atmospheric temperature (magnitude) to produce a change in the S_{diff}/S_{avg} signal equivalent to that produced by a 1-ppmv change in the CO_2 (i.e., the equivalent change) as a function of the narrow bandpass filter position and the filter width (thin lines, right axis). This figure highlights spectral regions of minimum temperature sensitivity and shows that the regions of minimum sensitivity are wider with wider filter profiles.

the distributions of CO_2 over a period of a few years would greatly improve our ability to understand the carbon cycle and predict future climate change. However, satellite-based measurement of atmospheric CO_2 is a very difficult problem, due to the high sensitivity required to measure the small variations in atmospheric CO_2. In this paper, I have analyzed the sensitivity of a simple, nadir-viewing, satellite-based, gas-filter correlation radiometer (GFCR) tuned in the 6300- (1.6 μm) and 5000-cm^{-1} (2.0 μm) regions for measuring the atmospheric CO_2 column. The GFCR technique was chosen in this analysis as it is an extremely powerful remote sensing technology and has a long history of satellite-based remote sensing of atmospheric composition. The spectral ranges were chosen as they include a number of relatively ''weak'' CO_2 bands located within a regions of minimal H_2O absorption (water vapor windows). Also, for a nadir-viewing satellite instrument, the upwelling radiation on the sunlit side of the earth will be primarily solar, minimizing the sensitivity to atmospheric temperature and maximizing the sensitivity to CO_2 in the boundary layer.

Calculations of the GFCR sensitivities to the CO_2 column and interferences due to variations in the atmospheric temperature and water vapor content were performed as a function of the spectral position of a narrow bandpass filter. The hypothetical GFCR consisted of two paths: one with a gas cell (correlation cell) with a pathlength of either 10 m (6300 cm^{-1}) or 2 m (5000 cm^{-1}) of CO_2 at 100 kPa, and the other with no CO_2. It was found that spectral regions of strong sensitivity to the CO_2 column with minimum sensitivity to variations in the atmospheric temperature exist. In one of these regions, centered at 6367 cm^{-1}, the change in the GFCR S_{diff}/S_{avg} signal per ppmv of CO_2 was -6.24×10^{-5}. Therefore, SNR in the S_{diff}/S_{avg} signal of $\approx$16 000 is re-

TABLE 4. Sensitivities of the GFCR detectors.

Channel	NEP (W)	S_{avg} (W)	S_{diff} (W)	S_{diff}/S_{avg}	NSR (SNR)
CO_2 (6367 cm^{-1})	7.9×10^{-14}	7.6×10^{-8}	1.3×10^{-8}	0.167	8.8×10^{-6} (114 000)
CO_2 (4831 cm^{-1})	7.9×10^{-14}	5.3×10^{-8}	1.1×10^{-8}	0.214	9.8×10^{-6} (102 000)
O_2 (13 158 cm^{-1})	7.9×10^{-14}	8.9×10^{-8}	7.6×10^{-9}	0.0859	1.5×10^{-5} (67 000)

quired to measure the CO_2 column to a precision of 1 ppmv. In another selected region, at 4831 cm^{-1}, the change in the S_{diff}/S_{avg} signal per ppmv of CO_2 was -1.16×10^{-4} (SNR of ≈8600). Calculations of the sensitivity to the vertical distribution of CO_2 were also performed and have shown that these measurements are strongly weighted to the lower atmosphere.

An analysis of these sensitivities to interference by both temperature and H_2O vapor variations showed that the choice of the GFCR technique and the filter position minimized the sensitivity to both parameters. The changes in the S_{diff}/S_{avg} signal per degree Celsius and per percent relative humidity (RH) for the 6367 cm^{-1} GFCR were 8.3×10^{-7} and 1.1×10^{-6}, respectively. Therefore, the required precision levels in knowledge of the temperature and relative humidity are 74°C and 56%, respectively. Also, the changes in the S_{diff}/S_{avg} signal per degree Celsius and per percent relative humidity (RH) for the 4831-cm^{-1} GFCR were 1.85×10^{-6} and -8.8×10^{-6}, respectively. Therefore, the required precision thresholds in knowledge of the temperature and relative humidity are 63°C and 13%, respectively. Consequently, atmospheric temperature and water vapor profiles provided by weather forecast models would most likely provide adequate resolution for these measurements.

An analysis of the sources of uncertainty in the proposed CO_2 radiometer was performed and showed that the most important potential sources of error is knowledge of the surface altitude and/or pressure. The change in the S_{diff}/S_{avg} signal per meter surface altitude (or per kPa of surface pressure) was 2.89×10^{-6} m^{-1} (-2.64×10^{-4} kPa^{-1}) for the 6367-cm^{-1} GFCR, and 8.56×10^{-6} m^{-1} (-7.29×10^{-4} kPa^{-1}) for the 4831-cm^{-1} GFCR. Therefore, in order to achieve a precision of 1 ppmv in the CO_2 column concentration, the surface altitude (pressure) of the measurement must be known to a precision of 21.6 m (0.254 kPa) or 13.5 m (0.159 kPa) for the 6367- and 4831 cm^{-1} GFCRs, respectively.

To measure the surface altitude and/or pressure, I am proposing to measure the total column of atmospheric O_2 using a similar GFCR tuned to the O_2 A band at 13 100 cm^{-1} (760 nm). This measurement may also be used as a cloud detection mechanism. The hypothetical GFCR consisted of two paths: one with a pathlength of

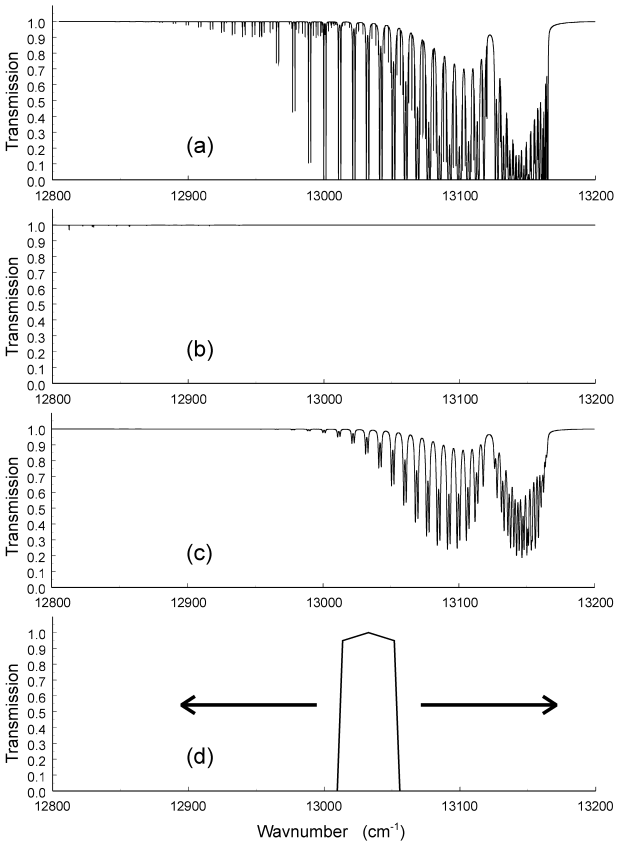

FIG. 17. Plots showing calculated atmospheric transmission spectra in the 12 800–13 200-cm^{-1} range of (a) O_2, (b) H_2O, (c) a 10-m-long gas cell filled with 1000 kPa of O_2, and (f) the transmission profile of a 42 cm^{-1} narrow bandpass filter used in this work. This calculation assumed a *U.S. Standard Atmosphere* (temperature and pressure), a relative humidity of 70% in the troposphere, and an SZA of 30°.

TABLE 5. Estimated resolution of GFCR channels assuming the following systematic errors: 10°C atmospheric temperature, 10% RH, and 10-m surface altitude.

	CO_2 GFCR (6367 cm^{-1})		CO_2 GFCR (4831 cm^{-1})		O_2 GFCR (13 158 cm^{-1})	
	Sensitivity	Error	Sensitivity	Error	Sensitivity	Error
CO_2 column sensitivity	-6.24×10^{-5} (ppmv CO_2)$^{-1}$	—	-1.16×10^{-4} (ppmv CO_2)$^{-1}$	—	0 (ppmv CO_2)$^{-1}$	0
Temperature sensitivity	8.30×10^{-7} (°C)$^{-1}$	8.30×10^{-6}	-1.85×10^{-6} (°C)$^{-1}$	1.85×10^{-5}	7.1×10^{-6} (°C)$^{-1}$	7.1×10^{-6}
Water vapor sensitivity	1.1×10^{-6} (% RH)$^{-1}$	1.1×10^{-5}	-8.84×10^{-6} (% RH)$^{-1}$	8.84×10^{-5}	0 (% RH)$^{-1}$	0
Surface altitude sensitivity	2.89×10^{-6} m^{-1}	2.89×10^{-5}	8.56×10^{-6} m^{-1}	8.56×10^{-5}	4.25×10^{-4} (20-m altitude)$^{-1}$	—
Instrument noise	—	8.8×10^{-6}	—	9.8×10^{-6}	—	1.7×10^{-5}
Sum of errors		3.3×10^{-5}		1.25×10^{-4}		1.84×10^{-5}
Estimated resolution of measurement		0.53 ppmv CO_2		1.1 ppmv CO^2		0.87-m altitude

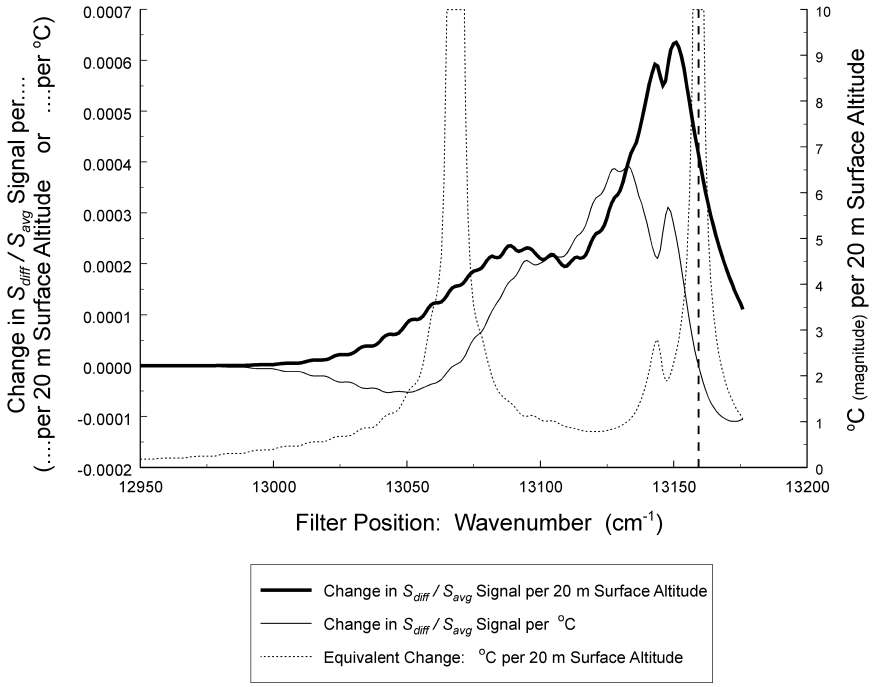

FIG. 18. Plot showing the change in the S_{diff}/S_{avg} signal as a function of (i) a 20-m change in the surface altitude (thick solid line, left axis) and (ii) a 1°C change in the atmospheric temperature (thin solid line, left axis), all as a function of the narrow bandpass filter position. Also shown is the required change in the atmospheric temperature (magnitude) to produce a change in the S_{diff}/S_{avg} signal equivalent to that produced by a 20-m change in the surface altitude (dotted line, right axis), also as a function of the narrow bandpass filter position (i.e., the equivalent change). This figure highlights spectral regions of minimum temperature sensitivity located in regions of strong sensitivity to changes in the surface altitude.

10 m of O_2 at 1000 kPa and the other with no O_2. Similarly, it was found that regions of strong sensitivity to the O_2 column with minimum sensitivity to variations in the atmospheric temperature exist. In one of these regions, centered at 13 158 cm^{-1}, the change in the S_{diff}/S_{avg} signal per 20 m of surface altitude was 4.25×10^{-4}. Therefore, an SNR in the S_{diff}/S_{avg} signal of $\approx$2500 is required to measure surface altitude to 20 m.

Calculations of the radiative sensitivity of the hypothetical CO_2 and O_2 GFCRs were performed. They showed that the expected NSRs in the 6367- and 4831-cm^{-1} GFCRs that may be achieved are 7 and 12 times lower than necessary, respectively, to measure the CO_2 column to a precision of 1 ppmv. Similarly, for the O_2 GFCR, the NSR that may be achieved is 28 lower than is necessary to measure the surface altitude to a precision of 20 m. As such, the sensitivities of the proposed GFCRs do not appear to be instrument limited.

Based on the sensitivity calculations performed, I have estimated the overall sensitivities of the hypothetical CO_2 and O_2 GFCRs. These estimates assumed that the sources of error, which include atmospheric temperature, water vapor, surface altitude, and instrument noise, are independent and random. They also assumed that the maximum systematic errors in the knowledge of the temperature, water vapor, and altitude were 10°C, 10% RH, and 10 m, respectively. I estimate that the overall sensitivities to the atmospheric CO_2 column of the 6367- and 4831-cm^{-1} GFCRs are 0.53 and 1.1 ppmv, respectively. Similarly, the overall sensitivity to the surface altitude of the 13 158 cm^{-1} O_2 GFCR is 0.8 m.

This paper is my first attempt to investigate the feasibility of satellite-based GFCR to remotely sound the atmospheric CO_2 column. Further analysis of the instrument design and sensitivities are needed before a full instrument proposal could be forwarded. However, this work has shown the great potential of a GFCR instrument in this endeavor, and has highlighted some of the challenges that must be overcome in designing such an instrument.

Acknowledgments. I would like to thank the Canadian Space Agency (CSA), the Meteorological Services of Canada (MSC), the Natural Sciences and Engineering Research Council of Canada (NSERC), Comdev International Ltd., and ABB Bomem Inc. for financial assistance in this research. I would also like to thank the following for their support: Jim Drummond, Kim Strong, Jinxue Wang, Dimitry Yashcov, Leonid Yurganov, Dany Plouffe, Phillipe Benoit, Matt Toohey, and Russ Alexander. This research was performed at the Department of Physics of the University of Toronto.

REFERENCES

Abel, P., P. Ellis, J. Houghton, G. Peckman, C. Rogers, S. Smith, and E. Williamson, 1970: Remote sounding of atmospheric temperature from satellites II. The selective chopper radiometer for Nimbus D. *Proc. Roy. Soc. London,* **320A,** 35–55.

Aoki, T., M. Fukabori, and T. Aoki, 1993: Trace gas remote sounding from near IR sun glint observations with tunable etalons. *High Spectral Resolution Infrared Remote Sounding for Earth's Weather and Climate Studies,* A. Chedin, M. T. Chedin, and N. A. Scott, Eds., NATO ASI Series, Vol. 19, Springer, 309–322.

Ciais, P., P. P. Tans, M. Trolier, J. W. C. White, and R. J. Francey, 1995: A large Northern Hemisphere terrestrial CO_2 sink indicated by the $^{13}C/^{12}C$ ratio of atmospheric CO_2. *Science,* **269,** 1098–1102.

Conway, T. J., P. P. Tans, L. S. Waterman, and K. W. Thoning, 1994: Evidence for interannual variability of the carbon cycle from the National Oceanic and Atmospheric Administration/Climate Monitoring and Diagnostics Laboratory Global Air Sampling Network. *J. Geophys. Res.,* **99,** 22 831–22 855.

Denning, A. S., I. Y. Fung, and D. Randall, 1995: Latitudinal gradient of atmospheric CO_2 due to seasonal exchange with land biota. *Nature,* **376,** 240–242.

Drummond, J. R., J. Houghton, G. Peskett, C. Rogers, M. Wale, J. Whitney, and E. Williamson, 1980: The stratospheric and mesospheric sounder on Nimbus 7. *Philos. Trans. Roy. Soc. London,* **296A,** 219–241.

——, G. P. Brasseur, G. R. Davis, J. C. Gille, J. C. McConnell, G. P. Peskett, H. G. Reichle Jr., and N. Roulet, 1993: MOPITT mission description documento Dept. of Physics, University of Toronto, Toronto, ON, Canada, 130 pp. [Available from Dept. of Physics, University of Toronto, Toronto, ON M5S 1A7, Canada; also available online at http://www.atmosp.physics.utoronto.ca/MOPITT/mdd_93/index.html.]

Ellis, P., and Coauthors, 1973: Remote sounding of atmospheric temperature from satellites IV. The selective chopper radiometer for Nimbus 5. *Proc. Roy. Soc. London,* **334,** 149–170.

Fan, S., M. Gloor, J. Mahlman, S. Pacala, J. Sarmiento, T. Takahashi, and P. Tans, 1998: A large terrestrial carbon sink in North America implied by atmospheric and oceanic carbon dioxide data and models. *Science,* **282,** 442–446.

Francey, R. J., P. P. Tans, C. E. Allison, I. G. Enting, J. W. C. White, and M. Trolier, 1995: Changes in oceanic and terrestrial carbon uptake since 1982. *Nature,* **373,** 326–330.

Houghton, J. T., G. J. Jenkins, and J. J. Ephraums, Eds., 1990: *Scientific Assessment of Climate Change—Report of Working Group I.* Cambridge University Press, 365 pp.

Keeling, C. D., R. B. Bacastow, A. F. Carter, S. C. Piper, T. P. Whorf, M. Heimann, W. G. Mook, and H. Roeloffzen, 1989: A three-dimensional model of atmospheric CO_2 transport based on observed winds, 1, Analysis of observational data. *Aspects of Climate Variability in the Pacific and the Western Americas, Geophys. Monogr.,* No. 55, Amer. Geophys. Union, 165–236.

——, J. F. S. Chin, and T. P. Whorf, 1996: Increased activity of northern vegetation inferred from atmospheric CO_2 measurements. *Nature,* **382,** 146–149.

Komhyr, W. D., R. H. Gammon, T. B. Harris, L. S. Waterman, T. J. Conway, W. R. Taylor, and K. W. Thoning, 1985: Global atmospheric CO_2 distributions and variations from 1968–1982 NOAA/GMCC CO_2 flask sample data. *J. Geophys. Res.,* **90,** 5567–5596.

Kuang, Z., J. Margolis, G. Toon, D. Crisp, and Y. Yung, 2002: Spaceborne measurements of atmospheric CO_2 by high-resolution NIR spectrometry of reflected sunlight: An introductory study. *Geophys. Res. Lett.,* **29,** 1716, doi:10.1029/2001GLO14298.

Kuze, A., H. Nakajima, M. Suzuki, and Y. Sasano, 2001: Measurement of greenhouse gases from space with a SWIR FTS. *Proc. SPIE,* **4485,** 69–80.

NOAA/CMDL/CCG, cited 2003: Carbon cycle greenhouse gases. [Available online at http://www.cmdl.noaa.gov/ccgg/.]

O'Brien, D. M., and P. J. Rayner, 2002: Global observations of carbon budget, 2, CO_2 column from differential absorption of reflected sunlight in the 1.61 μm band of CO_2. *J. Geophys. Res.,* **107,** 4354, doi:10.1029/2001JD000617.

——, R. M. Mitchell, S. A. English, and G. A. Da Costa, 1998: Airborne measurement of air mass from O_2 A-band absorption spectra. *J. Atmos. Oceanic Technol.,* **15,** 1272–1286.

Park, J. H., 1997: Atmospheric CO_2 monitoring from space. *Appl. Opt.,* **36,** 2701–2712.

Randerson, J. T., M. V. Thompson, T. J. Conway, I. Y. Fung, and C. B. Field, 1997: The contribution of terrestrial sources and sinks to trends in the seasonal cycle of atmospheric carbon dioxide. *Global Biogeochem. Cycles,* **11,** 535–560.

Rayner, P. J., and D. M. O'Brien, 2001: The utility of remotely sensed CO_2 concentration data in the surface source inversions. *Geophys. Res. Lett.,* **28,** 175–178.

Reichle, H., Jr., and Coauthors, 1986: Middle and upper tropospheric carbon monoxide mixing ratios as measured by a satellite borne remote sensor during November 1981. *J. Geophys. Res.,* **91,** 10 865–10 887.

——, and Coauthors, 1990: The distribution of middle tropospheric carbon monoxide during October 1984. *J. Geophys. Res.,* **95,** 9845–9856.

——, and Coauthors, 1999: Space shuttle based global CO measurements during April and October 1994: MAPS instrument, data reduction, and data validation. *J. Geophys. Res.,* **104,** 21 443–21 454.

Rothman, L. S., and Coauthors, 1998: The HITRAN molecular spectroscopic database and HAWKS (HITRAN atmospheric workstation): 1996 edition. *J. Quant. Spectrosc. Radiat. Transfer,* **60,** 665–710.

Tans, P. P., I. Y. Fung, and T. Takahashi, 1990: Observational constraints on the global atmospheric CO_2 budget. *Science,* **247,** 1431–1438.

Taylor, F. W., 1983: Pressure modulator radiometry. *Spectrometric Techniques,* G. A. Vanasse, Ed., Vol. 3, Academic Press, 137–197.

Tolton, B. T., and J. Drummond, 1999: Measurement of the atmospheric carbon monoxide column with a ground-based length-modulated radiometer. *Appl. Opt.,* **38,** 1897–1909.

——, and D. Plouffe, 2001: Sensitivity of radiometric measurements of the atmospheric CO_2 column from space. *Appl. Opt.,* **40,** 1305–1313.

——, M. Toohey, D. Plouffe, P. Benoit, and L. Yurganov, 2001: A concept for the remote sounding measurement of the atmospheric carbon dioxide column from space. *Proc. SPIE,* **4485,** 99–106.

Wofsy, S. C., and R. C. Harriss, 2002: The North American Carbon Program (NACP). Report of the NACP Committee of the U.S. Interagency Carbon Cycle Science Program, U.S. Global Change Research Program, Washington, DC, 56 pp.

Yang, Z., G. C. Toon, J. S. Margolis, and P. O. Wennberg, 2002: Atmospheric CO retrieved from space-based near IR solar spectra. *Geophys. Res. Lett.*, **29**, 1339, doi:10.1029/2001GLO14537.

Zimov, S. A., S. P. Davidov, G. M. Zimova, A. I. Davidova, F. S. Chapin III, M. C. Chapin, and F. J. Reynolds, 1999: Contributions of disturbance to increasing seasonal amplitude of atmospheric CO_2. *Science,* **284,** 1973–1976.